Design Embodiments Using Squeeze-Film Phenomenon to Attain Complete Separation of Contacting Surfaces

Cristinel Mares[1,*], Mark Atherton[1], Masaaki Miyatake[2] and Tadeusz Stolarski[1]

[1]*Department of Mechanical and Aerospace Engineering, College of Engineering, Design and Physical Sciences, Brunel University London, United Kingdom*
[2]*Department of Mechanical Engineering, Faculty of Engineering, Tokyo University of Science, Japan*
E-mail: cristinel.mares@brunel.ac.uk
[*]*Corresponding Author*

Received 03 June 2020; Accepted 26 August 2020;
Publication 27 November 2020

Abstract

In this paper four design embodiments that employ SFL to separate surfaces are explored. Section 2 details the fundamental principles of levitation based on SFL and associated Navier-Stokes equations. Section 3 describes four design embodiments utilising squeeze-film mechanism, namely a journal bearing, flexible frame, plain levitating plate and a non-contact gripper, in terms of their analytical description plus experimental and numerical results. Section 4 concludes the paper.

The paper demonstrates that the squeeze-film levitation is a feasible idea and can be implemented by a number of different embodiments. The mechanism of levitation is quite complex, and its computer modelling requires advanced numerical methods. All designs presented have been

European Journal of Computational Mechanics, Vol. 29_1, 83–114.
doi: 10.13052/ejcm2642-2085.2913

numerically modelled and the outcomes experimentally validated, which can be considered as the main contribution of this article.

Keywords: Squeeze-film mechanism, levitation mechanism, FEA, experimental analysis.

1 Introduction

There are many engineering situations in which two surfaces or objects must be separated to allow relative motion. Two common applications are bearing systems, where a load and/or relative motion between two parts is accommodated; and conveying systems where a stream of objects is transported along production lines [1]. Bearing systems using rolling elements or hydrodynamic/hydrostatic lubrication are well understood. Production line conveyors utilising rollers, belts, and chains in contact with the conveyed items are also well understood. However, there are a number of technologies for separating surfaces [2] in bearing systems and/or conveying that are less familiar in common engineering practice that are subjects for contemporary research into reducing surface wear, damage, friction and/or energy consumption.

Aerostatic non-contact transportation consists of air tracks and numerous orifices organised at appropriate intervals, which are utilised to produce non-contact levitation for objects through providing pressurised air beds via the orifices. An illustration of conveying of liquid crystal display (LCD) glass panels can be gleaned from the paper by Zhong et al. [3]. This method is expensive since a constant supply of a large quantity of compressed air and regular maintenance is necessary for the levitation.

The electrostatic levitator system (ESLS) was initially designed by Rhim et al. [4] at NASA's JPL lab. A charged item of 2 mm in diameter can be floated in a vacuum chamber between dual electrodes located vertically within an electrostatic field. The field is governed by a feedback system to preserve the levitated item at a predetermined location. A major drawback of the ESLS is that it needs either a high-vacuum or a high-pressure environment in order to supply a high electric field, which means it has limited applicability and in ambient air only small weights can be suspended. Alternately, a dielectric medium with a high electric field breakdown strength can be applied to suspend heavier items. Both the electrostatic force of attraction and plate weight scale linearly with the plate area, hence the voltage required to suspend the plate relies only on the plate thickness. For large plate thicknesses

and gaps, the voltage necessary becomes larger than the extreme voltage that can be supported without causing the electrical field to breakdown.

Magnetic Levitation System (MLS) has the capabilities to be used in industrial conveying. The literature reveals that several tons of load can be floated utilising MLS exemplified by full scale prototype trains operating in Japan and Germany [2]. The three main types of MLS are electromagnetic, electrodynamic, and Meissner's influence.

Electromagnetic levitation system (EMLS) is based on eddy currents induced in a conducting levitated item through applying a magnetic field. Mutual interaction between the eddy currents and the supplied magnetic field releases a levitation force. The force can be increased through suppling more current to the field windings. Materials that the EMLS can levitate are thus restricted mainly to electrical conductors ([5]. This approach is fundamentally unstable since the attraction is not robust for close proximity and consequently the item will become attached to the electromagnet system. A technique for stable electromagnetic levitation can be accomplished through including the electromagnet within an LCR (Inductance, Capacitance and Resistance) circuit adjusted such that if the item to be lifted moves away from the electromagnet the circuit growths the current and therefore increasing the force attracting the floating item. Contrariwise, if the levitated object transports toward the electromagnet the attraction force will weak. Consequently, through balancing the attraction force versus that of gravity, a stable levitation of the body can be achieved [6, 7].

In electrodynamic levitation, a good conductor suspended through repulsion by a magnetic field source. The magnetic field produces eddy currents in the conductor, and based on Lenz's Law, the eddy currents create a field which is against the external field. This fundamental effect provides stable levitation when a conductor is positioned above a magnetic field since the repulsion deteriorates with distance. The lifting height growths according to the magnitude of AC current applied. Two main applications of electrodynamic levitation are in high speed bearings and high-speed trains [8, 9].

In Meissner's effect levitation, suspension of a superconductor can be generated through repulsion of a magnetic field source. The repulsion occurs as superconductors eject a magnetic field from their cores [2, 7]. The item requires to be lifted must be cooled below their superconducting transition temperature. The magnitude of the critical temperature differs from material to material. As a result of which the item loses approximately all interior

magnetic flux. The method is stable, but providing a low temperature is an expensive method [2, 7].

Squeeze-film levitation is based on sound and proven fundamentals. In the field of micro-assembly, food, drug and semiconductor chip fabrication, precisely positioning and carrying delicate items is essential. The classical conveying process, which is generally based on mechanical contact, may contaminate and damage transporting objects. Traditional non-contact conveying technologies, like magnetic systems and air cushions, also creates various drawbacks in their applications such as particle accumulation [10–12]. Squeeze-film levitation (SFL) is anticipated to be an attractive contactless conveying technology since it has many advantages, for example, any material conductor or insulator, magnetic or non-magnetic, can be handled [13, 14]. The design of SFL can be as compact using a set of piezoelectric actuators attached to the underside a driving surface (thin plate). These distinct features make it appropriate for particular conditions where the compressed air or magnet sources for levitation and/or conveying are not applicable.

2 Fundamental Principles of Levitation Based on Squeeze-Film Phenomenon

The principle of squeeze-film is a promising technique to support an object on a thin air layer without using pressurised air. Reynolds equation is a partial differential equation governing the pressure distribution of thin viscous fluid film and is frequently used to model squeeze-film action. The general Reynolds equation is in the following form [15],

$$\frac{\partial}{\partial x}\left(\frac{\rho h^3}{12\mu}\frac{\partial p}{\partial x}\right)+\frac{\partial}{\partial y}\left(\frac{\rho h^3}{12\mu}\frac{\partial p}{\partial y}\right)=\frac{\partial}{\partial x}\left(\frac{\rho h\left(u_a+u_b\right)}{2}\right)+\frac{\partial}{\partial y}\left(\frac{\rho h\left(v_a+v_b\right)}{2}\right)+\rho\left(w_a-w_b\right)-\rho u_a\frac{\partial h}{\partial x}-\rho v_a\frac{\partial h}{\partial y}+h\frac{\partial \rho}{\partial t} \tag{1a}$$

In equation (1a), p is fluid film pressure, x and y are the bearing width and length coordinates, z is fluid film thickness coordinate, h is fluid film thickness, μ is fluid viscosity, ρ is fluid density, u, v, w are the bounding body velocities in x, y, and z directions respectively.

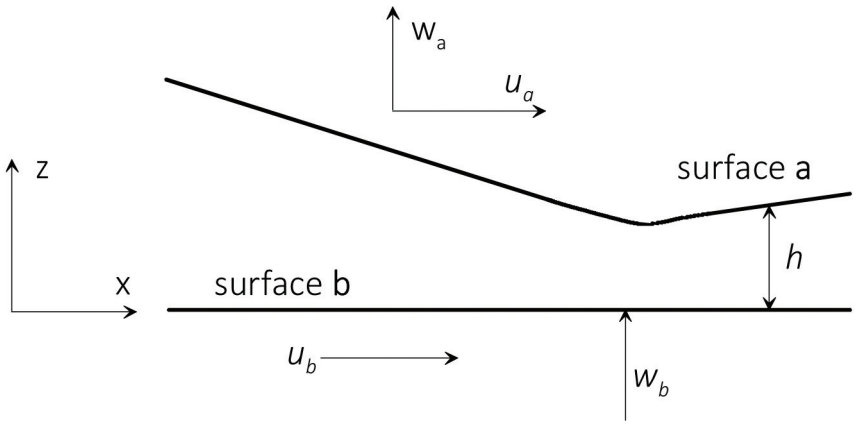

Figure 1 Normal squeeze and sliding velocities.

The Reynolds equation can either be used with consistent units or in the nondimensional form. The Reynolds equation assumes that the fluid is Newtonian, viscous forces dominate over inertia forces, fluid body forces are negligible and the variation of pressure across the fluid film is negligibly small, that is $\frac{\partial p}{\partial z} = 0$.

In case of different normal squeeze and sliding motions, schematically depicted in Figure 1, the Reynolds equation (1) is altered. If the density is assumed constant and the side leakage, represented by the second term on the left-hand side of equation (1), is neglected for simplicity, the Reynolds equation given by expression (1) can be rewritten as

$$\frac{\partial}{\partial x}\left(\frac{h^3}{12\mu}\frac{\partial p}{\partial x}\right) = \frac{u_a + u_b}{2}\frac{\partial h}{\partial x} + \frac{h}{2}\frac{\partial}{\partial x}\left(u_a + u_b\right) + w_a - w_b - u_a\frac{\partial h}{\partial x} \tag{1b}$$

Collecting terms gives,

$$\frac{\partial}{\partial x}\left(\frac{h^3}{12\mu}\frac{\partial p}{\partial x}\right) = \frac{u_b - u_a}{2}\frac{\partial h}{\partial x} + \frac{h}{2}\frac{\partial}{\partial x}\left(u_a + u_b\right) + w_a - w_b \tag{1c}$$

The right-hand side of the above equation (1b) shows that there are three distinct causes of pressure creation within a film existing between two interacting surfaces.

The first term, called "physical wedge" is responsible for pressure generation due to the flow of fluid through the narrow converging gap. Generation of

pressure postulated by the second term requires one of the interacting surfaces to contract or expand. The third term represents "pure" squeeze action and is responsible for creation of a lift force.

Generation of the levitation phenomenon is thus based on physical wedge and squeeze-film mechanisms and both are incorporated into the Reynolds equation.

The principal requirement for an effective squeeze film action consists in ensuring that there is displacement motion normal to interacting surfaces. The squeeze-film mechanism is considered to be one of the fundamental problems in fluid dynamics [16], and the Reynolds equation was used to analyse viscous flow enforced by squeeze action. Additionally, Tipei [17] and Salbu [18] examined distribution of pressure and resulting load capacity in a configuration consisting of two parallel coaxial discs. Beck [19] studied formation of a gas film between two circular flat surfaces. Analytical and experimental results generated by Takeda [20] during studies on non-parallel plates, parallel rectangular plates, and spherical bearing ought also to be mentioned. Transient Reynolds equation and transient motion equation of rigid bodies are usually utilised to find out load capacity magnitude created by squeeze-film action.

Basically, the equations governing squeeze-film action are derived from the Navier-Stokes equations. It is a normal practice to neglect higher order terms representing small quantities and to make the following simplifying assumptions:

(i) inertia forces are small in comparison to the viscous forces.
(ii) pressure within the film is constant through its thickness; (iii) the fluid under consideration is Newtonian. Having the simplifying assumptions in mind, one can express the pressure term and viscous term in the Navier-Stokes equations.

3 Design Embodiments Utilising Squeeze-Film Mechanism

3.1 Journal Bearing

Embodiment of the bearing able to change its geometry under the action of PZTs is shown in Figure 2 as a computer graphics image of actual bearing tested.

Bearing shown in Figure 2 had nominal diameter of 30 mm, 2 mm thickness of the wall, and 50 mm length. The radial clearance was set to 20 μm. The overall shape of the bearing is relatively simple and easy to make.

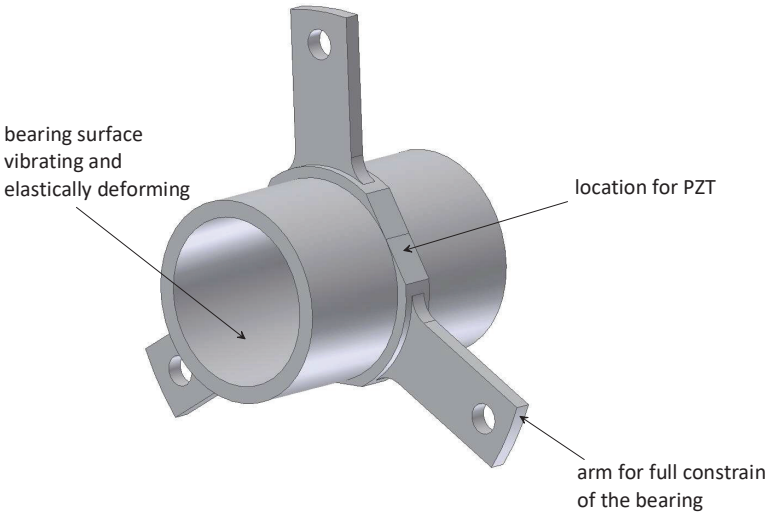

Figure 2 Image of the bearing experimentally tested.

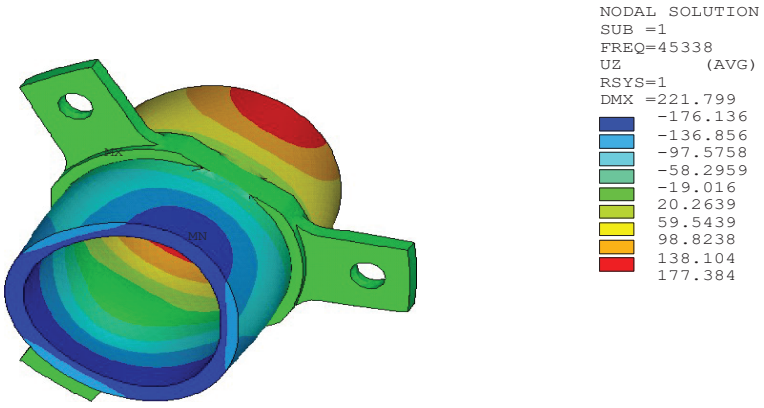

Figure 3 Finite element analysis of bearing elastic deformations.

Aluminium alloy was used to make the bearing because of its low coefficient of elastic strain energy absorption. At the locations indicated in Figure 2 three PZTs of the foil type were attached. They dimensions were, length – 12 mm, width – 10 mm and thickness – 0.5 mm. Due to the forces generated by PZTs, the bearing shell was deformed within elastic limit as shown in Figure 3. The image created by finite element analysis corresponds to the offset voltage of 60V applied to the PZTs.

First of all, it is easy to observe that the deformed shape of the bearing is very similar to that of three-lobe bearing commonly regarded as effectively improving dynamic stability of lightly loaded, high-speed air bearings. Furthermore, it has to be said that the elastic deformation of the bearing bore is relatively small and equal to 0.123 μm for the applied offset voltage of 60 V. Measurements of the lift magnitude (synonymous with separation of the shaft from the bearing surface) were carried out for the case of stationary shaft using a contactless probe. Sufficient number of repeated measurements were applied, and error involved was within $\pm 10\%$.

Determining an analytical model of a journal bearing operating on the squeeze-film based levitation requires incorporation of time dependent term in the Reynolds equation. By integrating the continuity equation across the squeeze-film thickness the following differential form of the Reynolds' equation is arrived at:

$$\frac{\partial q_x}{\partial x} + \frac{\partial q_y}{\partial y} + \frac{\partial (\rho h)}{\partial t} = 0 \tag{2}$$

where q_x and q_y are mass flow rates per unit length in the Cartesian coordinate system. Noting that in a deformed stage the bearing circular bore acquires three-lobe shape, the air film thickness, with reference to Figure 4, can be described by the following expression,

$$h = C_r + x_{cg} \sin\theta + y_{cg} \cos\theta + c(\theta, z, t) \tag{3}$$

The last term in equation (3) represents contribution of the bearing's bore cyclic deformation to the overall air film thickness.

C_r represents radial bearing clearance, c is a radial bearing bore deformation due to the action of PZTs, x_{cg} and y_{cg} denote shaft's centre instantaneous position.

Employing cylindrical co-ordinates, mass flow rates involved in the Reynolds' equation assume the forms,

$$q_\theta = \left(-\frac{h^3}{12\eta} \frac{p}{RT} \frac{\partial p}{r_0 \partial \theta} + \frac{r_0 \omega_1}{2} \frac{p}{RT} h \right) \Delta z \tag{4}$$

$$q_z = \left(-\frac{h^3}{12\eta} \frac{p}{RT} \frac{\partial p}{\partial z} \right) r_0 \Delta\theta \tag{5}$$

$$a_t = \frac{1}{RT} \frac{\partial (ph)}{\partial t} r_0 \Delta\theta \Delta z \tag{6}$$

Consequently, the analytical model of the squeeze-film bearing requires assembling equations which describe motion of the shaft centre. This is

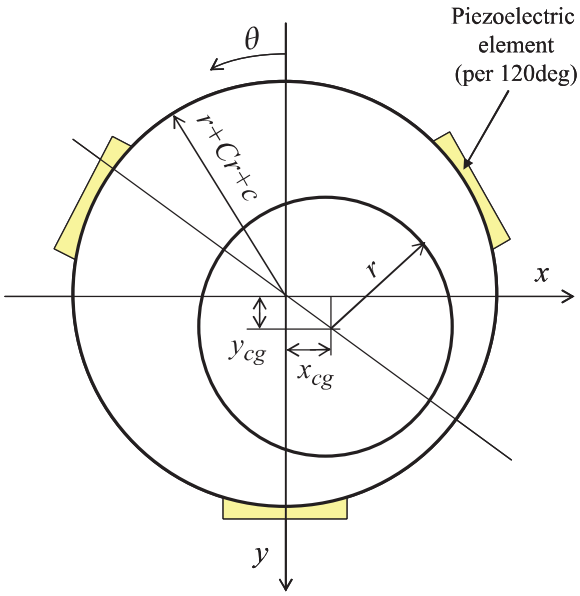

Figure 4 Schematic representation of the bearing's geometry.

achieved using the non-linear orbit method introduced by Castelli and Elrod [21] describing the shaft's motion in two mutually perpendicular directions as,

$$m\frac{d^2x_{cg}}{dt^2} = r_0\int_0^b\int_0^{2\pi} p\cos\theta d\theta dz \tag{7}$$

$$m\frac{d^2y_{cg}}{dt^2} = r_0\int_0^b\int_0^{2\pi} p\sin\theta d\theta dz + f_y \tag{8}$$

where $f_y = mgsin\varphi$ is the force acting on the bearing.

The equations of shaft motion are solved with the help of the Crank-Nicolson numerical procedure. Employing continuity of flow over a unit domain and using finite difference method, distribution of pressure with an air film is calculated and hence separation gap between the shaft and bearing bore at a given load is determined. The convergence limit was set to in the order of 10^{-6}.

Figure 5 shows the test results together with output of numerical calculations. The vertical axis denotes the distance between the shaft and the bearing at a given load indicated on the horizontal axis. All measurements

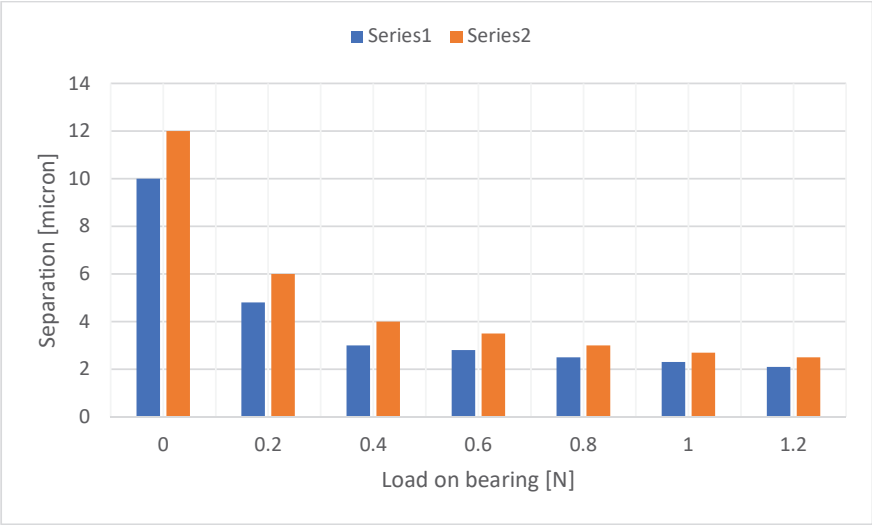

Figure 5 Separation of the shaft from inner bearing surface as a function of applied load Series 1 – calculated separation. Series 2 – measured separation.

were carried out at the frequency of bearing shell elastic deformations (case of PZTs switched on) equal to 58.3 kHz and the nominal radial clearance of 20 μm.

At the maximum load on the bearing (1.2 N), the separation is very small, although still feasible. Also, a reasonable agreement between measured and calculated separation can be seen, although measured separations are always greater than those calculated. This discrepancy presumably results from the simplification assumed in the analytical model of the bearing and indicates that a better more refined analytical model is required.

3.2 Flexible Frame

Another design embodiment capable of generating squeeze-film action is shown in Figure 6. It is based on the concept of "elastic hinges" [22]. The test device was made of an aluminum alloy, and with the total mass of 232g. The frame slides on a stationary 29.95×29.95 mm square guide while the inner dimensions of the bearing are 30×30 mm. This results in a nominal clearance of 50 μm. Because of a relatively large clearance, the upper film provides main contribution to levitate the frame. The side films have negligible effects on load capacity of the device but help to stabilize the frame's movement.

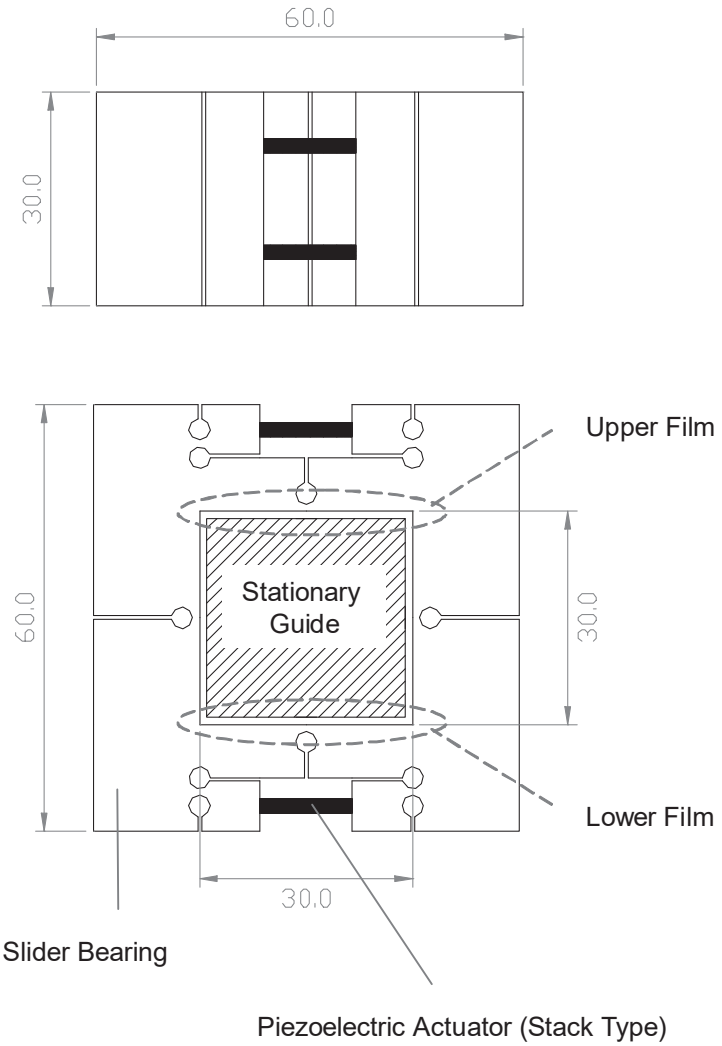

Figure 6 Schematic representation of flexible frame linear motion bearing.

As can be seen in Figure 6 the frame is equipped with 4 PZTs mounted in the slots of the bearing (2 in each slot). With applied voltages, the piezoelectric actuators expand and exert a load onto the bearing. The configuration of the elastic hinges is designed to generate the change in the clearance in a controllable manner. Figure 7, being an image created by the fine element analysis, shows the frame in the deformed state.

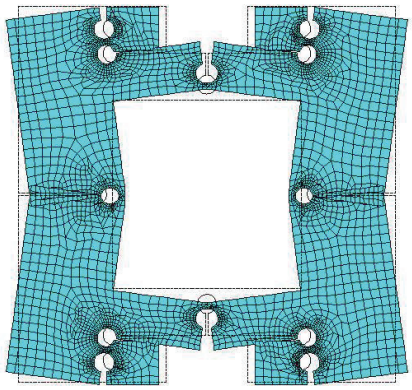

Figure 7 FE image of flexible frame in deformed state.

The size of the static clearance can be controlled accurately by the offset voltages (D.C.) applied to the piezoelectric actuators. It is estimated that 75V input gave an offset clearance of 8 μm. By imposing an oscillating (A.C.) voltage on the offset voltage, the bearing clearance will oscillate at a frequency and amplitude corresponding to that voltage. With sufficient amplitude and frequency, squeeze film pressure is generated between the bearing and the stationary guide to levitate the bearing to a floating height.

To reduce computational time, only the upper film of the frame was analyzed as it is the main source of load capacity. This is shown in Figure 8 for the upper part of the flexible frame.

The time dependent film thickness with its boundary conditions is defined by Equations (9a) and (9b).

For $0 \leq x \leq l_o/2$.

$$H = \frac{h}{h_m} = 1 + \left[\frac{h_{av}}{h_m} + \frac{h_a}{h_m}\sin(\omega t)\right]\left[\frac{x}{\frac{l_o}{2}}\right] \tag{9a}$$

For $l_o/2 \leq x \leq l_o$

$$H = \frac{h}{h_m} = 1 + \left[\frac{h_{av}}{h_m} + \frac{h_a}{h_m}\sin(\omega t)\right]\left[2 - \frac{2x}{l_o}\right] \tag{9b}$$

The isothermal compressible squeeze film pressure is described by the Reynolds equation is shown in Equation (10) in its non-dimensional form.

$$\frac{\partial}{\partial X}\left[PH^3\frac{\partial P}{\partial X}\right] + \frac{\partial}{\partial Z}\left[PH^3\frac{\partial P}{\partial Z}\right] = \sigma\frac{\partial(PH)}{\partial t} \tag{10}$$

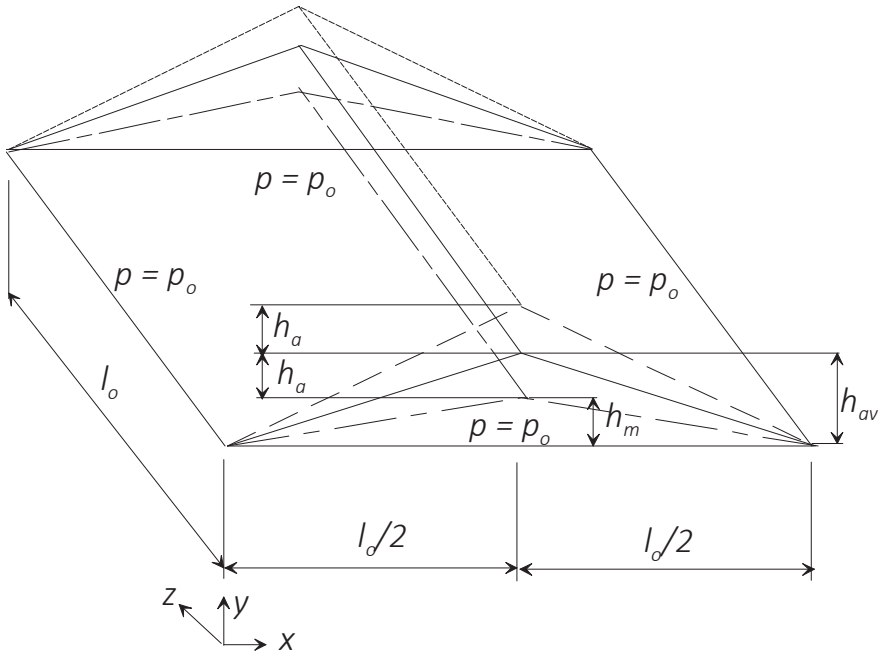

Figure 8 Schematic of the flexible frame upper part for analytical model.

where

$$\sigma = \frac{12\mu\omega l_o^2}{p_a h_m^2}$$

is the squeeze number.

Also, μ is the viscosity of a fluid, ω is frequency of the squeeze motion, h_m is the minimum film thickness, h_a is the amplitude in film thickness change, h_{av} is the average film thickness, h is the running film thickness, and t denotes time.

Finite difference method was applied to solve Equation (10) implicitly for predefined film thicknesses. The nonlinearity of Equation (10) was treated using the Newton-Raphson method and solved using the over-relaxation technique. Due to periodicity at steady state, it is only necessary to solve for one cycle. The film thicknesses were determined from the experiments and applied as input parameters for the theoretical analysis, this gave a direct comparison between the measured and the theoretical pressure profile.

Using ANSYS commercial CFD software numerical, results from the Reynolds equation solved with the help of the Newton-Raphson algorithm

were validated. Squeeze-film pressure generation was computed with the help of ANSYS CFX module.

Numerical simulation of the flexible frame was carried out in two main parts – FE dynamic structural analysis and CFX fluid flow analysis. The main objective of the FE dynamic structural analysis (ANSYS MPDL module) was to determine dynamic motion of the upper part of the frame caused by the piezo action. A file of dynamic motion (.csv format) was created and fed to the CFX fluid flow analysis as its input thus establishing the air film existing in the gap created between elastically deformed frame and the rigid guide. Since the gap changes in a cyclic way with frequency prescribed by piezo action, therefore unstructured two-dimensional mesh (Delauney algorithm) was used to continuously modify the grid. At the set-up step of the second stage of modelling, establishing realistic boundary conditions enable clear and concise simulation results. Thus, the standard properties of air were used. Velocity of air flow in the converging gap, created due to an elastic deformation of the frame, was linked to the frequency of oscillations produced by the PZTs. The residuals in Fluent are used to determine if the solution converges. The residuals plots were used to check if the solution had levelled off or had a steady decrease after a substantial number of iterations. In order to produce accurate results, it is essential that the convergence graph for each residual drops below 10^{-4} but remains above 10^{-6}. Residuals that did not converge required troubleshooting which called on optimisation of the mesh to a finer degree. Results produced by the simulation were reviewed in the post-processing stage.

Figure 9 shows the comparison between mid-plane peak-peak pressures solutions obtained from CFD and the Reynolds equation. However, for large vibration amplitudes or very thin film thickness, the Reynolds equation deviates away the CFD results, estimating a larger load capacity, expressed in Figure 9 as dimensionless pressure. Confidence in the use of Reynolds equation for squeeze film pressure solution is restricted to low load capacity applications. Squeeze film bearings generally operate with small vibrating amplitudes and hence justifies the use of Reynolds equation for this field of study. Rather large discrepancy between CFD and the Reynolds equation results is probably due to differences in shape and size of the air gap. In CFD simulation, shape and size of the gap is determined by the FE analysis and, therefore, more realistically reflect elastic deformation of the frame under given load generated by the PZTs. On the other hand, in the Reynolds solution, rather idealistic and linear change in the shape and size of the air

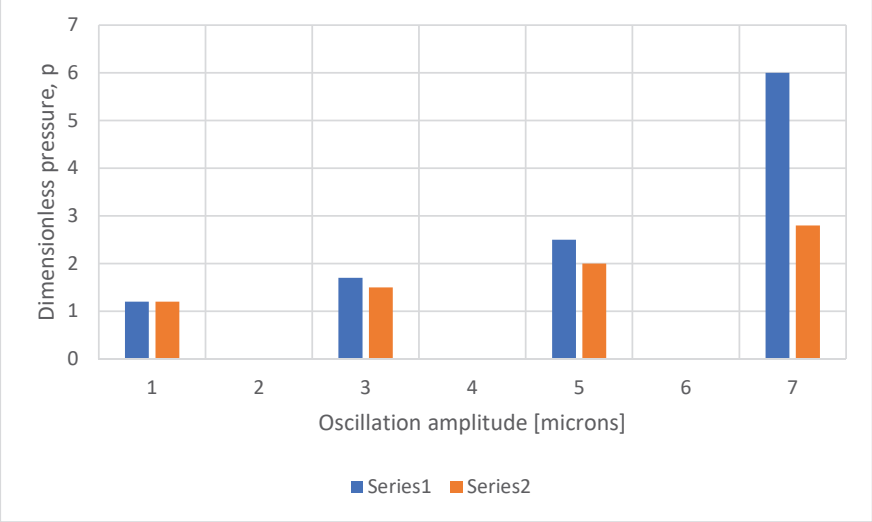

Figure 9 Dimensionless air film pressure as a function of frame's deformation amplitude. Series 1 – Reynolds equation results. Series 2 – CFD results.

gap is arrived at through a simple geometrical analysis of the triangular air gap shape.

Experimental results show that an oscillating film pressure in generated at steady state operation of the bearing, as shown in Figure 10. It was experimentally found that below 600 Hz, insufficient film pressure was generated for amplitude voltage of 25 V and above 2500 Hz, the power to the piezoelectric actuators is limited by the amplifier. The large peak-peak pressure around 732 Hz suggests that it is the first resonance mode, and maybe another one at high frequency not identified experimentally due to the amplifier limitations. It can be seen that the effect of resonance for frequencies 1100 Hz to 1700 Hz is negligible, where the response of the amplitude and film thickness agrees linearly with the input voltage. From that frequency range, it was determined that oscillating amplitudes of 25 V, 45 V and 65 V corresponds to amplitudes of 1 μm, 2.5 μm and 3.7 μm respectively. The floating height was also estimated to be 0.4 μm, 3 μm and 7 μm respectively. The above film thickness measurements of this predictable range were applied as input parameters the numerical scheme, where the pressure solutions can be directly compared to the measured film pressure.

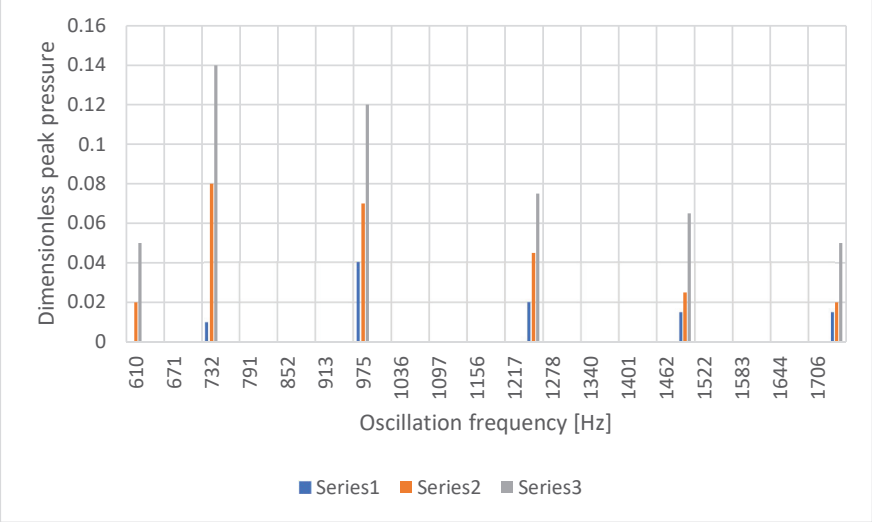

Figure 10 Dimensionless peak pressure in the air film as a function of deformation frequency. Series 1 – amplitude voltage 25V. Series 2 – amplitude voltage 45V. Series 3 – amplitude voltage 65V. Offset voltage – 75V.

3.3 Plain Plate

The essence of the third design embodiment able to induce squeeze-film action is based on the fact that a thin plate subjected to a uniaxial load creating plane stress will deform in the direction perpendicular to the applied load, which is known as the Poisson's contraction effect. The size of the dimple and its depth are both controlled by the magnitude of applied load, geometry of the plate and mechanical properties (Young's modulus and Poisson's ratio) of the plate's material. The shape of the dimple is such that it conforms to the requirement of the squeeze-film mechanism, that is when a planar and light object is placed on the plate at the location of the dimple the gap converging in the direction of fluid (air) flow is created. Figure 11 schematically illustrates the concept of the system. In order to initiate squeeze-film action the dimple has to be cyclically excited. This can be implemented through the use of piezo-electric transducers (PZT actuators). Oscillation of the dimple, created by Poisson's effect, is forcing the fluid (air) entrapped within the gap existing between the plate and floating object to flow outside and inside in accordance with cyclic deformation of the plate. However, under steady-state conditions established between pulsating dimple and the planar

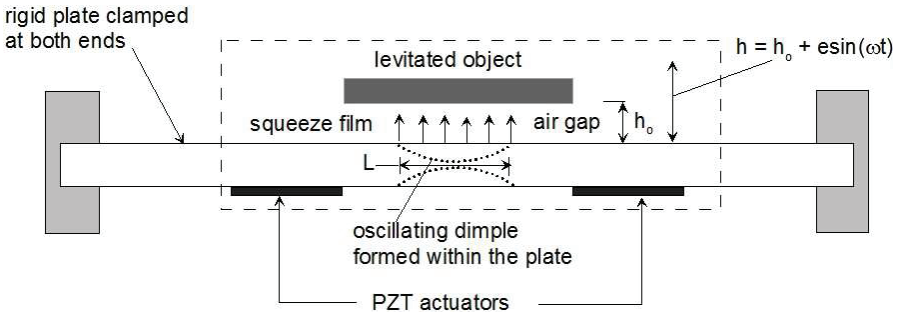

Figure 11 Schematic essentials of the levitation mechanism based on Poisson's contraction.

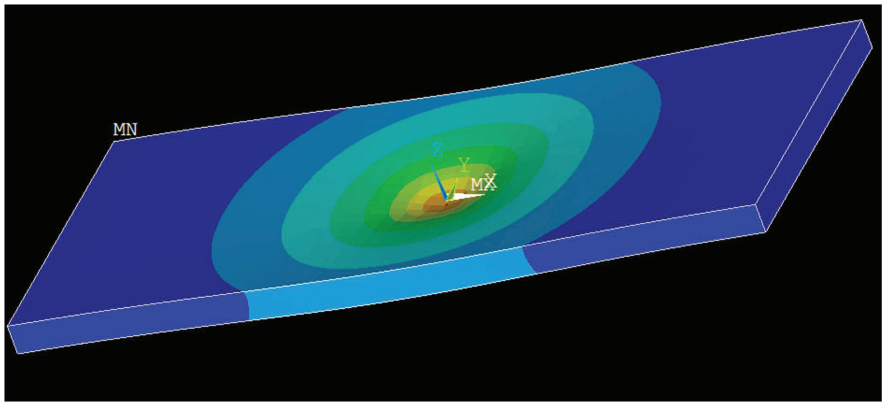

Figure 12 Computer image of the plate with a dimple created due to Poisson's contraction.

object, the average pressure within the air film is greater than the ambient pressure.

Figure 12 shows, for illustration purposes, an image create by the finite element analysis depicting a centrally positioned dimple and suggesting that the levitation is only possible just above the dimple and nowhere else over the plate's surface.

This simplified description of the squeeze-film action leading to levitation of a light, planar object is involving only centrally positioned dimple. However, experimental observations suggest that in reality something more complex is happening as the planar object levitates above the plate not only at the location of the central dimple but also all over the plate's surface. Figure 13 shows schematically the essential parameters controlling squeeze-film generated levitation [23]. The pressure (p) within squeeze-film space

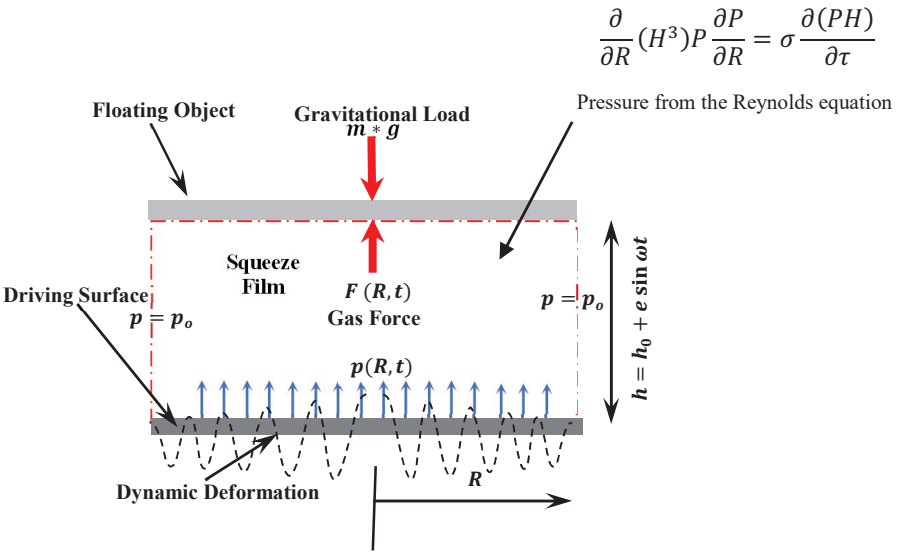

Figure 13 Schematic presentation of squeeze-film levitation – free body diagram.

is controlled by the Reynolds equation. Thus, the squeeze-film process is described by the Reynolds equation which describes pressure within the air film and the equation of motion which governs motion of the plate with mass (m).

The Reynolds equation can be expressed in the following form.

$$\frac{\partial}{\partial x}\left(\frac{\rho_a h^3}{12\mu}\frac{\partial p}{\partial x}\right) + \frac{\partial}{\partial x}\left(\frac{\rho_a h^3}{12\mu}\frac{\partial p}{\partial y}\right) = \frac{\partial}{\partial x}\left(\frac{\rho_a h\left(u_x + u_x'\right)}{2}\right) + \frac{\partial}{\partial y}\left(\frac{\rho_a h\left(u_y + u_y'\right)}{2}\right) + \frac{\partial\left(\rho_a h\right)}{\partial t} \tag{11}$$

Where, ρ_a is the air density, h is the squeeze-film height and μ is the fluid viscosity, t is time. The time dependent term $\frac{\partial(\rho_a h)}{\partial t}$ is identified as the "squeeze term" representing the squeezing movement of the fluid. In addition, u_x, u_y and u_x', u_y' refer to surface velocity components of bottom and top surfaces in x and y direction, respectively.

Introducing a perturbation factor for pressure of the order of ϵ into the Reynolds equation proposed by Langlois [24] one can obtain the squeeze-film force. It represents the force developed due to the pressure variations

within the squeeze-film space at a given instant of time.

$$\frac{\partial}{\partial R}\left(RH^3P\frac{\partial P}{\partial R}\right) = R\sigma\frac{\partial\, PH}{\partial T} \tag{12}$$

The boundary conditions of squeeze-film for a circular plate are:

$$\mathrm{P}(R, T=0) = 1 \tag{13}$$

The initial pressure between driving plate and levitating object is atmospheric. At the outer periphery,

$$\mathrm{P}(R=1, T) = 1 \tag{14}$$

$$\sigma = 12\mu R_0^2\omega/p_0h_0^2 \tag{15}$$

and, σ is the squeeze number.

Modelling the squeeze-film process requires coupling forces acting on the system that is fluid-structure domain. The coupling involves the Reynolds equation and the equations describing the motion of levitating object. They can be written as,

$$m\frac{d^2z_t}{dt^2} = F_f - F_m \tag{16}$$

$$F_f = \iint (p_j - p_0)rdrd\theta \tag{17}$$

$$_m = mg \tag{18}$$

where F_f represents the fluid flow force which is generated due to the variation of pressure and F_m is the weight of the floating object. Using $z = h_0Z, p = p_0P$, and $\tau = t\omega$ it is possible to transform equation (17) into dimensionless form, where, h_0 is initial clearance, p_0 is an ambient pressure, ω is the frequency of oscillations.

$$\frac{d^2Z}{d\tau^2} = \frac{p_0r_0^2}{mh_0\omega^2}\iint (P_j - 1)RdRd\theta - \frac{mg}{mh_0\omega^2} \tag{19}$$

$$z_t = z_l + h \tag{20}$$

Differentiation of Equation (20) with respect to time produces;

$$\frac{d^2z_t}{dt^2} = \frac{d^2z_l}{dt^2} + \frac{d^2h}{dt^2} \tag{21}$$

The height of levitation, z_l can be expressed as $z_l = Z_0 \sin\tau$, thus;

$$\frac{d^2 z_l}{dt^2} = -\omega^2 Z_0 \sin\tau \tag{22}$$

In a normalised form Equation (22) assumes the following appearance,

$$\frac{d^2 Z}{d\tau^2} = -\omega^2 Z_0 \sin\tau + \frac{d^2 H}{d\tau^2} \tag{23}$$

Substitution of Equation (23) into Equation (19) results in the following expression;

$$-\omega^2 Z_0 \sin\tau + \frac{d^2 H}{d\tau^2} = \frac{p_0 r_0^2}{m h_0 \omega^2} \iint (P_j - 1) R dR d\theta - \frac{mg}{m h_0 \omega^2} \tag{24}$$

or

$$\frac{d^2 H}{d\tau^2} = \frac{p_0 r_0^2}{m h_0 \omega^2} \iint (P_j - 1) R dR d\theta + \omega^2 Z_0 \sin\tau - \frac{mg}{m h_0 \omega^2}$$

Equation (24) is a second-order nonlinear partial differential equation and its initial conditions $(t = 0)$ are given as $\frac{dH}{dT} = 0$ $P_n = 1$.

A numerical simulation utilising ANSYS CFX was used to examine the performance of levitating an object in the form of a 35 mm diameter disc with mass of 5 g. The behaviour of the system, simulated by CFX, is described by Equation (24). However, in view of easy availability of the CFX software, there was no attempt to solve Equation (24) although it could be solved using, for instance, the Newton-Raphson method mentioned earlier. Only a one degree of freedom model was constructed to determine height of levitation in the vertical direction. From a physical point of view, the instantaneous position of the floating object is defined by equilibrium of its inertia, the fluid flow force created by pressure distribution within the air gap formed between the floating disc and the driving plate, and gravitational force. Three boundary conditions, named as Top, Bottom, and Side, were established. The Top boundary condition refers to the bottom surface of the floating disc and also represents the mass of the disc. The Bottom boundary condition denotes the top surface of the driving plate and also the bottom plane of the air film which is modelled as a deforming boundary. A displacement amplitude was assigned to the Bottom boundary to create a squeeze action in the vertical direction. Finally, the Side boundary was treated as an open boundary, that is the air flow through this boundary was not restricted.

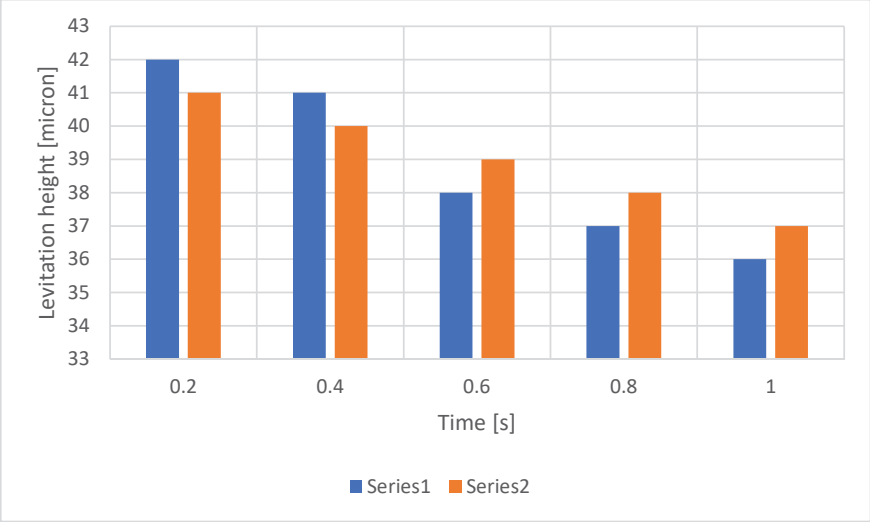

Figure 14 Comparison of experimental measurement with CFX simulation for the plate of design C (see Table 1). Series 1 – computational; Series 2 – experimental.

Numerical simulation of the plain plate performance consisted of two main parts – FE dynamic structural analysis and CFX fluid flow analysis. The main objective of the FE dynamic structural analysis was to determine dynamic motion of the dimple formed in the driving plate due to the Poisson's contraction caused by the piezo action. A file of dynamic motion (.csv format) was created and fed to the CFX fluid flow analysis as its input thus establishing the air film existing in the gap. Next, meshing was created, initial and boundary conditions were applied, and equations of motion controlling the movement of the floating disc written. The solution stage was initiated by imposing convergence conditions. The final outcome of the CFX analysis was the examination of the disc's motion and pressure distribution in the air film using post-processing facilities of the CFX software.

The results of the numerical model and experimental measurements generated for the plate of design C (see Table 1) are plotted together in Figure 14.

It is apparent that there is a slight difference in predicted and measured levitation height. On average, the difference between CFX and experiment is around 5.3%. A number of factors might possibly contribute to that. Firstly, CFX predictions are not consistently exceeding measured results as evidenced by Figure 14. Therefore, there is need to conclude that CFX

Table 1 Configurations of the plate used during experimental testing

Design No.	Plate size mm	Material	Modulus of Elasticity GPa	Density kg/m^3	Poisson's Ratio
A1	200x100x0.5	Aluminium	69	2676	0.33
A2	200x100x1				
A3	200x100x2				
B	200x100x0.5	Stainless Steel	193	7781	0.33
C	200x100x2	Polyethylene High density (HDPE)	1.08	970	0.46

always overestimate the levitation height of the disc. Also, the time is an important factor as at the beginning of CFX simulation the amplitude of disc's motion is quite high and with the passage of time the motion of the disc stabilises as the equilibrium of forces acting on it is established. Additionally, inherent for numerical procedures rounding up should also be mentioned as a possible source of errors. On the other hand, experimental measurements will inevitably create some errors, such as noise of the electronic devices used (voltage amplifier and signal generator), and the accuracy of the laser sensor. Therefore, it might be justified to use a different numerical procedure than that offered by the CFX. One potential candidate for that could be the smoothed particles hydrodynamics (SPH) with efficient implementations using Python.

The importance of the plate design (see Table 1 for details of five different designs used) for the levitation height is shown in Figure 15.

Since a laser sensor was used to measure the levitation height, it enabled management of the output data and therefore the height at which the floating object levitated for the designs examined is given as the average obtained from measurements of the laser sensor. It is apparent from Figure 15, that a steady state floating object height of 70 μm takes place for design A1 while levitation at height of 22.3 μm happens for design A3. It has to be pointed out that although the plate of design A1 and the plate of design A3 are both made of aluminium, nevertheless they have very different thicknesses. Plate A1 is four times thinner than plate A3. This fact points out the importance of using thin plates in order to avoid extra bending of the plate due to moments created by piezo action. This extra bending certainly diminishes the Poisson's contraction and hence reduces levitation height. The overall conclusion from the plate design point of view is that the levitation height is predominantly determined by material properties (Poisson's ratio coefficient) although thinner is the plate the better.

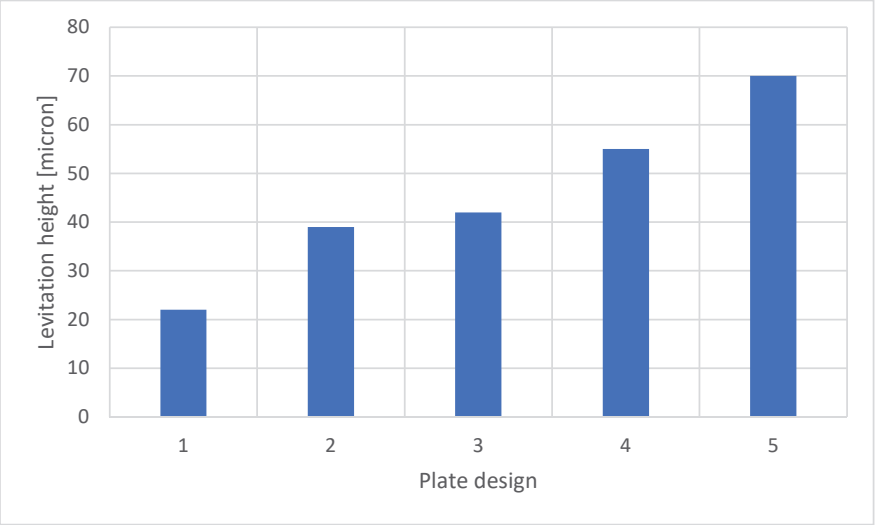

Figure 15 Measured levitation height in micron for various plate designs specified in Table 1. (1) – design A3; (2) – design B; (3) – design C; (4) – design A2; (5) – design A1.

3.4 Non-Contact Gripper Utilising Langevin Oscillator

The need to handle fragile and lightweight parts such as silicon wafers, optical lenses and human body tissues without physical contact creates a demand for non-contact grippers. One of the promising solutions to the problem is to use a chuck-type design utilising ultrasonic vibration, also called the squeeze chuck [25]. It has been found that when a nominally flat surfaces vertically vibrates with ultrasonic frequency then an object placed on the surface is subjected to both vertical (levitation) and horizontal (stability) forces [26]. Figure 16 depicts schematically the fundamental principle involved in creation of levitation in his design embodiment [27].

As a result of the vibration of the lower surface, the upper surface becomes separated from the lower one due to the pressure generated within the air film, which on average is larger than the atmospheric pressure. This phenomenon was experimentally investigated, using the experimental set-up shown in Figure 17 [27].

The gripper, in a form of a Langevin oscillator, was mounted on a frame and as a floating object a square shaped silicon chip was used. Both the height of levitation of the chip and the magnitude of the horizontal, stabilizing force were measured. The relationship between average floating height (h) and amplitude voltage (V_{amp}) applied to the oscillator is shown in Figure 18.

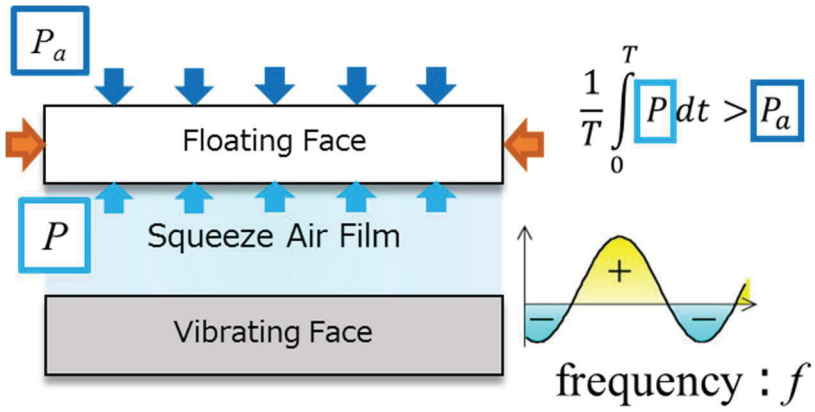

Figure 16 Schematic principle of the squeeze-film effect.

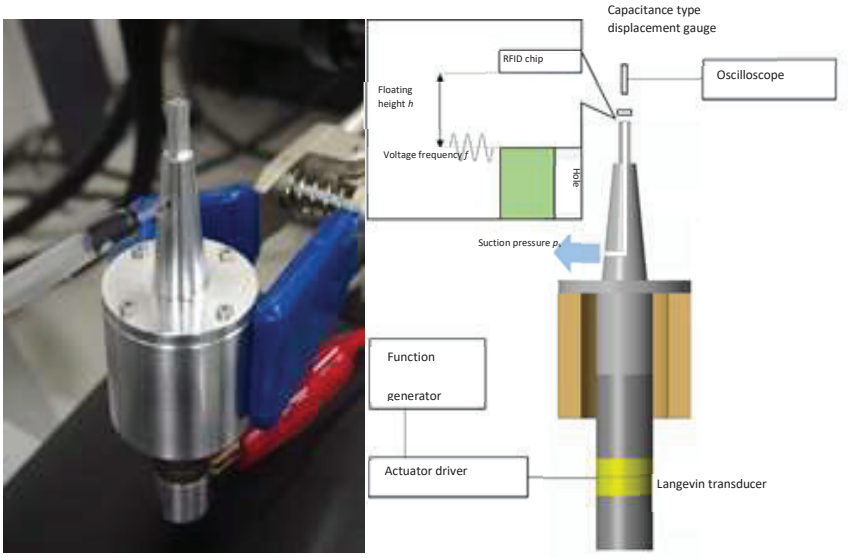

Figure 17 Schematic view and photograph of the experimental set-up.

It can be noticed that floating height increases almost linearly with amplitude voltage. Horizontal stabilizing force (F) as a function of the horizontal displacement (Δx) is presented in Figure 19.

The measurements were carried out for four different suction pressures applied to the floating object (chip) through a small hole drilled in the top part of the gripper attached to the Langevin oscillator. The rationale behind this

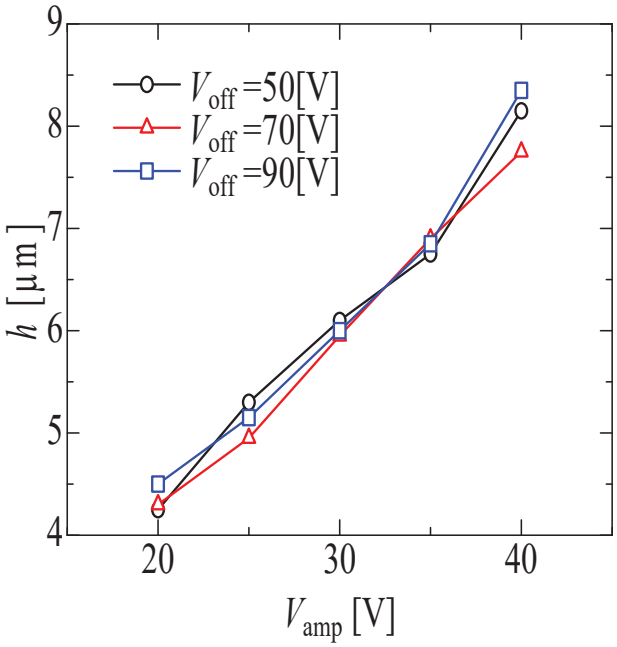

Figure 18 Relationship between V_{amp} and h.

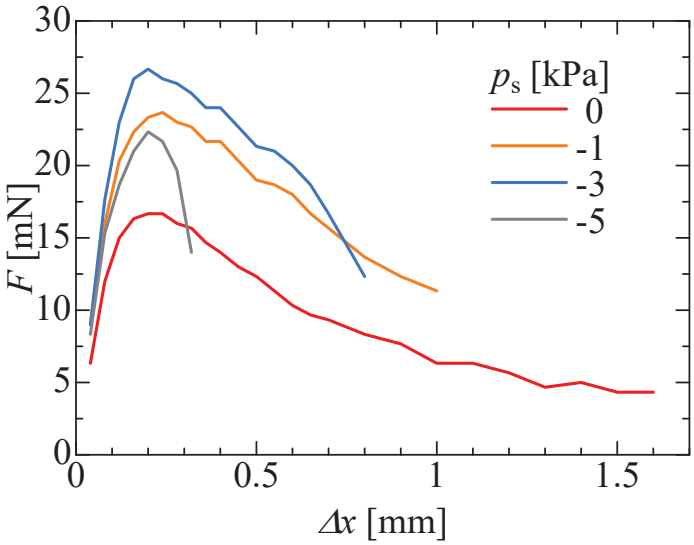

Figure 19 Relationship between Δx and F.

was an idea that the suction pressure might enhance the horizontal stabilizing force acting on the floating chip.

Experimental results unequivocally point to the practical usefulness of the con-contact gripper. However, at present there is no numerical model of the gripper enabling rapid and efficient examination of the role played by various factors of the gripper in its present embodiment. A promising way forward leading to a numerical model could be modification of the traditional Reynolds equation to include effects of inertia postulated by Stolarski and Chai [28]. The starting point for modification of the Reynolds equation ought to be Navier-Stokes equation in polar coordinates. For axisymmetric case, they are,

$$\rho\left[\frac{\partial u}{\partial t}+u\frac{\partial u}{\partial r}+w\frac{\partial u}{\partial z}\right]=-\frac{\partial p}{\partial r}+\mu\frac{\partial^2 u}{\partial z^2} \tag{25}$$

And

$$\frac{\partial p}{\partial z}=0 \tag{26}$$

If the fluid of concern is a compressible one and the conditions are isothermal than the equation of continuity is of the following form,

$$\frac{\partial p}{\partial t}+\frac{1}{r}\frac{\partial(rpu)}{\partial r}+\frac{\partial(pw)}{\partial z}=0 \tag{27}$$

Where u and w represent velocities respectively in r and z directions; z is normal to the air film, p is the pressure, and t denotes time.

As forces due to fluid viscosity govern the squeeze-film action, therefor the body forces can be conveniently ignored in the Navier-Stokes equation (25). The traditional Reynolds equation describing squeeze-film action between to discs of which one is levitating and the other one driving can be written as,

$$\frac{\partial(ph)}{\partial t}=\frac{1}{12}\frac{\partial(rph^3}{r\partial r} \tag{28}$$

where r is the radius of the disc and h is the temporary squeeze-film thickness.

However, when inertia effects are incorporated into the squeeze-film action than the modified Reynolds equation is arrived at.

$$\frac{\partial(ph)}{\partial t}=\frac{1}{12}\frac{\partial(rp\psi h^3)}{r\partial r} \tag{29}$$

where

$$\psi\left(r\right)=\frac{1}{120\mu hRT}\left[\frac{\partial\left(rp\psi^2h^5\right)}{r\partial r}-10\frac{\partial\left(r\psi h^3\right)}{\partial t}\right]+\frac{1}{\mu}\frac{\partial p}{\partial r} \tag{30}$$

In the expression (30), μ is the fluid viscosity, R is the universal gas constant, and T is the temperature in absolute units.

The squeeze motion and thickness of the air film are both included in the governing equation in the following way,

$$m\frac{\partial^2 z}{dt^2} = 2\pi \int_0^{r_0} (p - p_a)\, r dr - w \tag{31}$$

$$h = h_0 + s\,(r,\ t) + z(\tau) \tag{32}$$

In the above equations, (31) and (32), r_0 is the radius of both discs, h_0 is the initial thickness of the air film developed due to squeeze action, $s(r, t)$ represents transient modal shapes of the driving disc, p_a denotes atmospheric pressure, and w depicts gravitational force of levitating disc with mass m.

The above equation could be solved with the help of one of currently available numerical methods. This is currently being done and the results of numerical simulation of the non-contact gripper will be published in due course.

4 Conclusions

Performance results of four different design embodiments employing squeeze-film phenomenon to separate interacting surfaces by a thin air film thus creating non-contact situation justify the following conclusions.

1. All four embodiments are feasible for practical applications where contactless interaction between elements is critically required.
2. The magnitude of levitation height depends on the design embodiment, but all four designs demonstrate the ability to separate contacting surfaces by a thin film of air.
3. The first embodiment, journal bearing, is most suitable for applications in which rotational motion prevails.
4. The other two designs, that is flexible frame and plane plate, are ideal for linear conveying of light objects.
5. The fourth design is a novel type of a contactless gripper to be used in handling fragile and lightweight objects.
6. Analytical models produce results close to experimental measurement although the agreement between them is not always entirely satisfactory.
7. The use of the CFX numerical simulation software might be replaced by a different numerical method such as smoothed particles hydrodynamics

(SPH) in order to ascertain if SPH generates results closer to experimental measurements.

8. Levitation height of an object over the plane plate (driver), apart from Poisson's ratio coefficient of the material used, also substantially depends of the plate's thickness.

References

[1] McGuire, P.M., 2009. Conveyors: application, selection, and integration, 1st Edition, ISBN 9781439803905, CRC Press.

[2] Brandt, E.H., 1989. Levitation in physics. Science, 243(4889), pp. 349–355.

[3] Zhong, W., Li, X., Liu, F., Lu, D., Tao, G. and Kagawa, T., 2013. Modelling and experimental validation of dynamic characteristics of porous-walled air film for non-contact conveyor system. Proceedings of the Institution of Mechanical Engineers, Part J: Journal of Engineering Tribology, 227(7), pp. 787–797.

[4] Rhim, W.K., Chung, S.K., Barber, D., Man, K.F., Gutt, G., Rulison, A. and Spjut, R.E., 1993. An electrostatic levitator for high-temperature containerless materials processing in 1-g. Review of Scientific Instruments, 64(10), pp. 2961–2970.

[5] Wang, T.C. and Tzeng, Y.K., 1994. A new electromagnetic levitation system for rapid transit and high-speed transportation. IEEE transactions on Magnetics, 30(6), pp. 4734–4736.

[6] Taniguchi, N., Nanotechnology: Integrated Processing Systems for Ultra-Precision and Ultra-Fine Products, Oxford: Oxford University Press, 1996.

[7] Thangali, S.R., 1991. Noncontact handling of semiconductor wafers, mechanical engineering, master dissertation.

[8] Mak, S.Y. and Young, K., 1986. Floating metal ring in an alternating magnetic field. American Journal of Physics, 54(9), pp. 808–811.

[9] Mak, S.Y. and Young, K., 1986. Determination of the self-inductance of a metal ring. Physics Education, 21(2), p. 111.

[10] Liu, P., Li, J., Ding, H. and Cao, W., 2009. Modeling and experimental study on near-field acoustic levitation by flexural mode. IEEE transactions on ultrasonics, ferroelectrics, and frequency control, 56(12).

[11] Vandaele, V., Lambert, P. and Delchambre, A., 2005. Non-contact handling in microassembly: Acoustical levitation. Precision engineering, 29(4), pp. 491–505.

[12] Reinhart, G. and Hoeppner, J., 2000. Non-contact handling using high intensity ultrasonics. CIRP Annals-Manufacturing Technology, 49(1), pp. 5–8.
[13] Stolarski, T. A. and Chai Wei, 2006. Self-levitating sliding air contact. International Journal of Mechanical Sciences, 48(6), pp. 601–620.
[14] Shou, T., Yoshimoto, S. and Stolarski, T., 2013. Running performance of an aerodynamic journal bearing with squeeze film effect. International Journal of Mechanical Sciences, vol. 77, pp. 184–193.
[15] Hamrock, Bernard J., 1994. Fundamentals of Fluid Film Lubrication. McGraw-Hill.
[16] Dowson, D., 1999. History of tribology, New York, ASME.
[17] Tipei, N., 1954. Equatiile Lubrificatiei cu Gaze, 1954. Communicarile Academiei Republicii Populare Romane; vol. 4.
[18] Salbu, E. O. J., 1964. Compressible squeeze films and squeeze bearings. Transactions of ASME, Series D., Journal of Basic Engineering, vol. 86.
[19] Beck, J. V., 1969. Experiment and analysis of a flat disk squeeze film bearing including effects of supported mass motion. Transactions of ASME, Journal of Lubrication Technology, vol. 91.
[20] Takeda, H., 1983. Characteristics of squeeze air film between nonparallel plates. Transactions ASME, Journal of Lubrication Technology, vol. 105.
[21] Castelli, V. and Pirvics, J., 1968. Review of numerical methods in gas film analysis. Transactions ASME, Journal of Lubrication Technology, vol. 90, pp. 777–792.
[22] Stolarski, T. A. and Miyatake, M., 2018. Acoustic Journal Bearing with Changeable Geometry and Built-in Flexibility. Transactions ASME, Journal of Tribology, vol. 140.
[23] Stolarski, T. A., 2010. Numerical modelling and experimental verification of compressible squeeze film pressure. Tribology International, vol. 43, No. 1–2.
[24] Almurshedi, A., Atherton, M., Mares, C., Stolarski, T., 2019. Modelling influence of Poisson's contraction on squeeze film levitation of planar objects. Journal of Applied Physics, vol. 125.
[25] Langlois, W.E., 1962. Isothermal squeeze films. Quarterly of Applied Mathematics, Vol. XX, No. 2, pp. 131–150.
[26] Yamazaki, T., Yoshimoto, S. and Toda, K., 2007. Study on Non-contact Chuck Using Ultrasonic Effect, Proceedings of the Japan Society of Mechanical Engineers part C, 73(728), 1208–1214.

[27] Yoshimoto, S., Sekine, H., Miyatake, M, 2010. A non-contact chuck using ultrasonic vibration: analysis of the primary cause of the holding force acting on a floating object. Proceedings of the Institution of Mech. Eng., Part C: Journal of Mech. Eng. Sci., vol. 224, No. 2.
[28] Mita, K., Miyatake, M., Atherton, M., Mares, C., Yoshimoto, S., Stolarski, T., 2017. Non-contact handling equipment using ultrasonic vibration. Proceeding of the World tribology Congress, Beijing, China, September 17–22.
[29] Stolarski, T. A. and Chai Wei, 2008. Inertia effect in squeeze film air contact. Tribology International, vol. 41, pp. 716–723.

Biographies

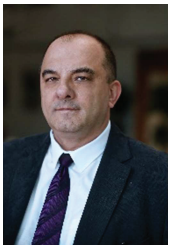

Cristinel Mares is Reader at Brunel University of London, Department of Mechanical and Aerospace Engineering, and a Fellow of the Institution of Mechanical Engineers. His research interests include structural dynamics, identification and optimization, structural health monitoring and condition monitoring, in particular acoustic emission and guided waves propagation.

Mark Atherton is Professor of Design Engineering at Brunel University of London and a Fellow of the Institution of Mechanical Engineers. He received

a BSc(Hons) in Mechanical Engineering from Aston University, Birmingham; MSc in Industrial Robotics and Automation from Imperial College, London; and PhD in Mechanical Engineering Design from City University, London.

Masaaki Miyatake received his B.Eng.,M.Eng. and Dr.Eng. from Tokyo University of Science in 2001, 2003,2006, respectively. He started his career as an assistant professor in 2006 at Tokyo University of Science. He joined Oiles corp. as an engineer from 2010 to 2013. In 2013, he started again his career at Tokyo University of Science as a Lecturer and promoted to an associate professor in 2016. His research interests include mechanical design, precision engineering and tribology, in particular fluid film bearings, non-contact floating devices and self-lubricated bearings using green materials.

Tadeusz Stolarski, MSc, PhD, DSc (Eng), DIC (Imperial College), CEng, FIMechE has an international reputation for his research in the field of tribology and surface mechanics. Based at Brunel University as professor in the Mechanical Engineering Department, he has widely published (over 130 peer reviewed papers) and four books as well as numerous conference presentations. He has also been acting as a technical advisor to a number of well-known companies.

His specific areas of expertise include:

He has progressed through all levels of academic positions at Brunel University London, including headship of mechanical engineering. Currently he holds appointment as a research professor at the Department of Mechanical Aerospace and Civil Engineering, College of Engineering, Design and Physical Sciences, Brunel University London and is actively involved in research on self-levitating sliding contacts.